

# Hybrid Simulations of Interstellar Pick-up Ion Acceleration at the Solar Wind Termination Shock

Sharadini Rath, P. C. Liewer, B. E. Goldstein,

*Jet Propulsion Laboratory, California Institute of Technology, Pasadena, CA 91109*

**Abstract** Hybrid (kinetic ion/fluid electron) simulations have been used to study self-consistently the acceleration of interstellar pick-up ions at the solar wind termination shock. Results are presented from 3D-dimensional simulations of high Mach number oblique (400-600) shocks with a 10% population of interstellar pick-up hydrogen. In these simulations, the pick-up ions, the solar wind ions, the shock fields and the waves are all treated self-consistently. Pick-up ions reflected by the shock excite large amplitude ( $\Delta B/B \sim 0.3$ ) upstream magnetosonic waves. These waves, in turn, scatter the pick-up hydrogen, as expected in the diffusive shock acceleration process. The spectrum of excited waves broadens in time. We find that, for the parameters studied, the termination shock efficiently accelerates the interstellar pick-up hydrogen. A study of accelerated pick-up ion orbits shows that the energy gain comes predominantly from shock drift acceleration in the shock front, with the waves aiding the acceleration by allowing multiple encounters with the shock. Results for the energetic ion fluxes are compared to predictions of diffusive shock acceleration theory and show qualitative agreement.

## Introduction

It has been hypothesized that anomalous cosmic rays (20-300 MeV) may result from the acceleration of interstellar pick-up ions at the solar wind termination shock [Pesses et al., 1981; Jokipii, 1986, 1990]. Interstellar pick-up ions enter the heliosphere as neutrals. They are ionized and picked up by the solar wind which carries them back out to the termination shock. The interstellar neutrals ( $\sim 20$  km/sec) have a large velocity relative to the solar wind ( $V_{sw} \sim 400$  km/sec) and hence these pick-ups have a much larger energy in the solar wind frame ( $\sim \frac{1}{2} m V_{sw}^2$ ) than the background solar wind ions. Thus, they form a natural higher energy "seed" population for acceleration at the termination shock. The

largest pick-up component is expected to be hydrogen, representing over 10% of the solar wind ion density if the termination shock is beyond 50 AU. Recently, Gloeckler et al. [1993] have made the first observations of interstellar pick-up hydrogen.

Ions are accelerated at collisionless shocks primarily by two processes [see reviews Forman and Webb, 1985 and Jones and Ellison, 1991]: shock drift acceleration and first order Fermi acceleration. In shock drift acceleration, an ion gains energy due to the drift generated by the gradient in the magnetic field at the shock and the resultant electric field. In this process, the ion travels along the shock front and gains energy continuously. In first order Fermi acceleration, an ion gains energy by scattering between converging magnetic fluctuations upstream and downstream of the shock. For parallel shocks, with no average jump in the magnetic field at the shock, Fermi acceleration is expected to dominate, whereas in more oblique or quasi-perpendicular shocks, shock drift acceleration is expected to dominate [Jokipii, 1987]. Much of the work on ion acceleration at shocks uses the standard convection-diffusion cosmic ray transport equation which contains both of these effects [Jokipii, 1982, 1990; Jones and Ellison, 1985]. In such work, the macroscopic fields and the diffusion coefficient, which includes the wave scattering, are specified and an assumed energetic seed population is "injected." The theory is valid only for isotropic distribution functions and particles with velocities much greater than any convective speeds in the problem and thus cannot be used to model the acceleration of the freshly picked up interstellar ions.

Here, we use the complementary technique of hybrid particle simulation to study the acceleration of freshly picked up interstellar ions at the solar wind termination shock. Self-consistent hybrid simulations have been used previously by Giacalone et al. [1992, 1993] and Scholer [1990] to study the acceleration of thermal ions in parallel or nearly parallel shocks ( $\theta_{Bn} < 20^\circ$  where  $\theta_{Bn}$  is the angle between the magnetic field and the shock normal). We have extended this previous work to study the acceleration of the energetic pick-up ion "seed" population in oblique ( $\theta_{Bn} = 40^\circ - 60^\circ$ ) shocks. In addition, we have

studied the evolution of the spectrum of the upstream waves generated self-consistently by the reflected pick-up ions; no upstream waves are injected.

### Simulation Model and Parameters

The hybrid simulation model used here, as well as the assumed termination shock parameters, have been described in Liewer et al. [1993]. The code is based on the hybrid model of Winske and Leroy [1985]. For the studies here, the code was modified to include a second ion species, the interstellar pick-up ions, which are initialized with a spherical shell distribution in velocity space. For simplicity, we assume a spherical shell velocity distribution with zero width and a radius equal to the solar wind velocity co-moving with the solar wind ions. The angle of the termination shock itself will be highly variable [Liewer et al., 1993]; we chose  $\theta_{Bn} = 400\text{-}600$  degrees because for these angles the field is parallel enough to allow reflected ions to move back up stream and excite waves and the field is perpendicular enough to have a significant jump in the magnetic field at the shock to make shock drift acceleration important. Also, for these oblique angles, parallel diffusion is more important than perpendicular diffusion so that the absence of cross-field diffusion does not invalidate the simulation model [Jokipii et al., 1993]. The simulation is done in the downstream frame. Ions are injected from the left of the simulation box and reflect off the right wall. The shock forms at the right wall and propagates to the left. Reflected ions that reach the left wall are absorbed. In the simulations below,  $\omega_{pi}/\omega_{ci} = 7000$ ,  $\beta_e = 0.5$ ,  $\beta_i = 0.2$ , and the fractional density of the pick-up hydrogen is  $n_0^P/n_0 = 10\%$  where  $n_0$  is the initial total density and  $n_0^P$  is the initial hydrogen pick-up ion density. These numbers, plus the angle and Mach number, characterize the shocks completely and represent values expected for a solar wind termination shock at  $\sim 80$  AU [Liewer et al., 1993].

The code uses dimensionless units with length normalized to  $c/\omega_{pi}$  where  $\omega_{pi}$  is the ion plasma frequency ( $\omega_{pi}^2 = 4\pi n_0 e^2/m_p$  with  $m_p$  the proton mass), and velocities are normalized to  $c$ . Variation is allowed only in the  $x$  (shock propagation) direction and the magnetic field is in the  $y$ - $z$  plane. The simulation of acceleration to high energies requires

very large simulations. The computation were performed using 32 processors of the 512 processor Intel Delta Touchstone parallel computer at Caltech and ran about 12 hours. Typical runs had a time step of  $0.025 \omega_{ci}^{-1}$ , a system length of  $3500 c/\omega_{pi}$  with 7000 grid points and 1 million particles and ran for 20,000 time steps. For solar wind parameters at about 80 AU, the time step corresponds to about 6 sec and  $c/\omega_{pi} \approx 7000$  km.

### Simulation Results

We will present results from two case studies, characterized by the angle  $\theta_{Bn}$  between the magnetic field and the shock normal, and the Alfvén Mach number  $M_A$  (the ratio of the solar wind speed to the Alfvén speed). Case 1 has  $\theta_{Bn} = 40^\circ$  and  $M_A = 5$ ; Case 2 has  $\theta_{Bn} = 50^\circ$  and  $M_A = 8$ . In both simulations, as the shock propagates, the interstellar pick-up hydrogen ions are preferentially reflected by the shock as reported previously [Liewer et al., 1993]. A counter streaming instability between these reflected pick-up ions and the background solar wind leads to large amplitude upstream magnetosonic waves. The pickup ions are observed to be further accelerated in these shock and waves fields. The waves and turbulence are generated by the shock, i.e., no waves are injected upstream.

Case 1 ( $\theta_{Bn} = 40^\circ$  and  $M_A = 5$ ) Figure 1 shows results from the lower Mach number Case 1 at times early and late in the simulation. Figure 1a shows results at  $t = 150 \omega_{ci}^{-1}$ . In the top panel, the magnetic field component  $B_y(x)$  vs.  $x$  (with  $B$  normalized to the upstream magnetic field magnitude  $B_0$ ), shows a large amplitude upstream magnetosonic wave with peak amplitude  $\Delta B_y/B_0 \approx 0.5$ . The second panel shows pick-up ion  $V_x$  vs.  $x$  phase space with only every 60th ion plotted. In this panel, the injected pick-up ion “shell” is seen as the band of ions centered on  $v_x/c = 5 \times 10^{-3}$ ; some reflected pick-ups are evident as those with negative  $V_x$ . The third panel shows “energetic/reflected” pick-up ion phase space  $V_x$  vs.  $x$ , where “energetic/reflected” pick-ups are *upstream* ions with energy greater than 4 times the initial energy in the solar wind frame ( $E_0 = \frac{1}{2} m_p V_{sw}^2$  where  $V_{sw}$  is the solar wind speed); all such ions are plotted. The magnetosonic wave structure seen in the  $B_y$  plot is clearly evident in the energetic/reflected ion phase space,

confirming that it is indeed the reflected pick-up ions which are driving the upstream instability. These waves propagate upstream at roughly the Alfvén speed, but are convected back towards the shock by the  $M_A = 5$  solar wind flow. In Fig. 1 b ( $t = 550\omega_{ci}^{-1}$ ), the  $y$  component of the magnetic field  $B_y(x)$ , the total magnetic field amplitude  $|B(x)|$ , and "energetic/reflected" pickup ion phase space  $V_x$  vs.  $x$  are shown. The wave amplitude is comparable to the value at the earlier time, but the waves appear to be much less monochromatic. Moreover, the energetic ion phase space shows much less structure, and higher energy ions are evident, indicating that nonlinear wave-scattering processes are playing a significant role.

Figure 2 shows the magnetic fluctuation spectra  $P(k) = B^2(k)/8\pi$  vs  $k$ , (with  $k$  in units of  $\omega_{pi}/c$ ) at the same two times as in Fig. 1 integrated over a region extending  $1024 c/\omega_{pi}$  ahead of the shock. At the early time, the spectrum is peaked around the value  $ck/\omega_{pi} \approx 0.12$ . This is consistent with theoretical expectations for the beam-driven ion cyclotron instability which predicts  $\omega - \mathbf{k} \cdot \mathbf{V}_b = k_{par}(V_A - V_b) = -\omega_{ci}$ . The beam velocity along the field, determined from plots of the reflected ion  $v_{perp}$ - $v_{par}$  phase space, is  $V_b/V_A \approx 12$ . With  $k = k_{par}/\cos\theta_{Bn}$ , the predicted value is  $ck/\omega_{pi} \approx 0.12$  as observed. At later times, the spectrum has clearly broadened, with more energy going into longer wavelength modes. The broadening of the spectral peak around 0.12 presumably results from the broadening of the reflected pick-up ion beam observed in the reflected/energetic ion phase space in Fig. 1 b, with the longer wavelength modes excited by the more energetic pick-up ions.

In order to understand better the shock acceleration process and the relative role of wave scattering and shock drift acceleration, "orbits" of the most energetic ions were plotted. Two typical ion orbits are shown in Fig. 3 where an individual ion's energy (in the solar wind frame) is plotted as a function of its distance from the shock front  $x - x_{shock}$  (negative values are upstream) where  $x$  is normalized to  $c/\omega_{pi}$ . Here  $E = v^2/c^2$  (e.g., energy is normalized to  $m_p c^2/2 = 4.5 \times 10^8$  keV) and the initial pick-up ion energy is  $E_0 = 5 \times 10^{-7}$  (corresponding to 220 eV). The ion position and energy at the start of the simulation are at

the bottom left end of the orbit curve. This type of plot clearly shows the energy gain from shock drift acceleration: the ion stays in the shock front ( $x - x_{\text{shock}} \approx 0$ ) and gains energy continuously. Wave scattering causes the observed abrupt decreases in energy because the waves are propagating away from the shock and the reflected ions are overtaking the waves. (In some cases, wave scattering causes an increase in energy, indicating that some backward propagating waves have been excited.) From investigation of the orbit plots, we concluded that both processes, wave scattering and shock drift acceleration, are important in accelerating pick-up ions at the termination shock. Wave scattering is important because it allows the ions to have multiple encounter with the shock; the actual energy gain comes from the shock electric field [Jokipii, 1982, 1987, 1990; Jones and Ellison, 1985].

From the study of 65 orbits of the most energetic ions in Case 1, we found that acceleration resulted primarily from shock drift acceleration at the shock front, where the energy gained from shock drift acceleration in a single encounter was often much greater than the gain from simple specular reflection by the shock. Scattering from upstream waves was the dominant mechanism for returning ions to the shock front, with downstream waves playing a smaller role. In many cases, ions stayed quite near to the shock (within  $\sim 100 c/\omega_{pi}$  or  $5-20 \rho_i$  where, in our units,  $\rho_i = \omega_{pi}/\omega_{ci} \approx 13^{1/2} \approx 7000 E^{1/2}$ ) and shock drift acceleration led to large energy gains (up to 20 times their original energy) in only a few such encounters with the shock. In some of these cases, the ions were kept near the shock by scattering and the very large magnetic fluctuations near the shock front, evident in Fig. 1 b, probably play a major role. The plot on the left in Fig. 3 is one such orbit. At the first encounter with the shock, the ion moves nearly along the shock front gaining energy from shock drift acceleration to  $E = 4 \times 10^{-6}$ . It then moves upstream about  $120 c/\omega_{pi} \sim 14 \rho_i$  where it is then scattered back to the shock for a second encounter and energy gain. In about 60% of the cases, the ions gained their energy in one or two such encounters. In the other  $\sim 40\%$  of the cases studied, the ions moved a larger ( $> 100 c/\omega_{pi}$ ) distance from the shock before being scattered back or the energy gain came for three or more encounters.

An orbit of this type is shown on the right in Fig. 3. The ion has gained 24 times its original energy, corresponding to an increase from 220 CV to 5 keV.

The energetic particle flux resulting from the acceleration processes and the diffusive shock theory predictions (straight lines) are shown in Fig. 4 for both Case 1 and Case 2 (below). Plotted is the differential energy flux  $dJ(E)/dE$  of the energetic/reflected ions ( $E = v^2/c^2$ ) in a region ( $x\omega_{pi}/c = 0-1800$ ) upstream of the shock. For Case 1, many ions have been accelerated to  $E > 10^{-5}$  (corresponding to  $> 5$  keV), which represents an increase of more than 20 times the initial pick-up ion energy of  $E_0 = 5 \times 10^{-7}$ . Also shown is the slope of the flux predicted by diffusive shock theory

$$\frac{dJ(E)}{dE} \propto E^{-\alpha} \quad \text{with} \quad \alpha = \frac{r+2}{2(r-1)},$$

where  $r$  is the compression ratio of the shock. This power law is expected to be valid, independent of the shock angle [Jones and Ellison, 1991]. Averaging crudely over the large fluctuation at the shock front, the observed ratio for Case 1 (cf. Fig. 1 b) is  $r \approx 2.5$  giving  $\alpha = 1.5$ . Diffusive shock theory makes no prediction of the magnitude of the differential flux. Moreover, diffusive shock theory is strictly applicable only for isotropic distribution functions and particles with velocities much higher than the convective velocities, and these conditions are certainly violated for the pick-up ion distributions in the simulation.

The above diffusive theory prediction is for the flux behind the shock, whereas we have plotted the upstream flux. The flux from the simulation has additional spatial and temporal variations folded into the curve, but the simulated flux is more or less consistent with the predicted slope in the mid-energy range where the additional variations are less important. Diffusive shock theory predicts that the upstream density of energetic ions should decay exponentially with distance from the shock front with the decay length increasing with ion energy [see review by Forman and Webb, 1985]. This was studied in the simulation of Giacalone et al. [1993] and, qualitatively, has been observed in these simulations as well. The much more rapid fall off of the simulation flux than the diffusive theory prediction may be partially due to the folding in of this spatial dependence and, in

addition, partially due to the finite length and time of the simulation. Higher energy particles have a longer scattering mean free path and take longer systems and times to accelerate them.

Case 2 ( $\theta_{Bn} = 50^\circ$  and  $M_A = 8$ ) For this case with  $\theta_{Bn} = 50^\circ$  and  $M_A = 8$ , the shock is much stronger and the ion energies are corresponding larger. However, many aspects are similar to Case 1. Figure 5 shows, for a time late in the simulation, the y component of the magnetic field  $B_y(x)/B_0$ , the total magnetic field strength  $B(x)/B_0$  and the "energetic/reflected" pick up ion density  $n_{ref}^P$  (as defined above), normalized to the upstream pick-up ion density  $n_0^P$ . The upstream waves have a somewhat larger amplitude as expected for this higher Mach number shock with more energetic pick-up ions. Note that some of the waves have steepened into "shocklets." Very large amplitude ( $\Delta B/B_0 \approx 8$ ) waves are also evident just downstream of the shock. The "energetic/reflected" density is shown to illustrate the efficiency of the shock acceleration process. In the region just upstream of the shock, the density of the energetic/reflected pick-up ions is very high (10%-30% of the incident pick-up ion energy). We attempted to quantify the "injected" population by fitting an exponential curve to the energetic/reflected population, excluding the variable region at the front. The energetic ion density in the region to the left of  $x = 2000$   $c/\omega_{pi}$  can be parameterized roughly as  $n_{ref}^P(x)/n_0^P \approx 0.05 \exp[(x-2000)/\lambda]$  where  $\lambda \approx 1700(\pm 200) c/\omega_{pi}$ . Thus, about 5% of the pick-up ions are injected into the acceleration process.

The energetic particle flux  $dJ(E)/dE$  resulting from the acceleration processes and the diffusive shock theory prediction for Case 2 is shown in the right half of Fig. 4. It can be seen that, relative to Case 1, the higher Mach number led to not only an upward shift in bulk energy, but also a dramatic widening of the flux in the intermediate energy range. This broadening results from a slower fall off in energy, consistent with the prediction of diffusive shock theory. For this case the observed overall shock compression ratio (not including the overshoot) was  $r \approx 3.5$  (cf. Fig. 5) giving  $\alpha = 1.1$ . In the mid-energy range,

the observed flux is consistent with the diffusive prediction although. as above, the flux from the simulation has additional spatial and temporal variations folded into the curve. In this case, the initial pick-up ion energy was  $E_0 = 1.3 \times 10^{-6}$  (~0.6 keV). Many ions have been accelerated to  $E > 6 \times 10^{-5}$  (~30 keV), representing a 50-fold increase in energy.

Figure 6 shows the magnetic fluctuation spectra  $P(k) = B^2(k)/8\pi$  vs  $k$ , (with  $k$  in units of  $c/\omega_{pi}$ ) at two times in the simulation,  $t\omega_{ci} = 150$  and 500, again integrated over a region extending  $1024 c/\omega_{pi}$  ahead of the shock. At the early time, the spectrum is peaked in the region  $ck/\omega_{pi} \approx 0.07-0.09$ . This is consistent with predictions for the beam-driven ion cyclotron instability for the observed reflected beam velocity of  $V_b/V_A \approx 18-22$ . At later times, the spectrum has clearly broadened, with more energy going into longer wavelength modes as observed for Case 1 (Fig. 2). The broad enhancement in the spectral region  $ck/\omega_{pi} \approx 0.02--0.1$  is presumably driven by the higher energy reflected pickup ions accelerated by this  $M_A = 8$  shock.

Figure 7 shows the orbits of two of the most energetic pick-up ions from Case 2, energy (normalized to  $m_p c^2/2$ ) versus distance from the shock (in units of  $c/\omega_{pi}$ ). Both ions have been accelerated to about 50 times their initial energy ( $E_0 = 1.3 \times 10^{-6}$  or -0.6 keV) to about 30 keV. A study of 65 of the orbits of the most energetic ions for this case led to the same conclusions as for Case 1, e.g., the acceleration resulted primarily from shock drift acceleration in the shock front with the upstream waves aiding the processes by returning the ions to the shock for multiple encounters. Scattering, from downstream waves was less important. Many ions studied appear to remain trapped near (within  $100 c/\omega_{pi}$ ) the shock front (either by the fluctuations or the DC fields), acquiring their energy (via shock drift acceleration) in a small number of encounters with the shock, As in Case 1, in about 60% of the orbits studied, the ions had only one or two such encounters with the shock. In the orbit on the left in Fig. 7, the energy gain comes from shock drift acceleration in two “encounters” with the shock. The ion on the right gains its energy from about 4 encounters with the shock.

## Summary and Discussion

We have used a hybrid simulation model to show that interstellar pick-up hydrogen ions can be effectively accelerated at the solar wind termination shock for oblique shock angles. The hybrid simulation model allows a self-consistent treatment of the shock fields, the solar wind and pick-up ions and the waves and turbulence. Reflected pick-up ions drive the strong upstream turbulence needed to support diffusive shock acceleration. At early times in the simulation, the spectrum is peaked at the mode expected for a reflected-ion-beam-driven ion cyclotron instability and the pick-up ion phase shows a well defined reflected beam. As the simulation progresses, the spectrum broadens in time with energy going to longer wavelengths as the pick-up ions are accelerated and non-linear wave scattering becomes important. For strong shocks ( $M_A = 8$ ), many ions were accelerated to 50 times their initial energy, representing an increase from 0.6 keV to 30 keV for the parameters used.

A study of orbits of the most energetic pick-up ions shows that the primary mechanism of energy gain is shock drift acceleration at the shock front, with the waves allowing the ions to make multiple encounters with the shock. The energy gained via shock drift acceleration in a single encounter can be much greater than that gained from simple specular reflection from the shock front. In many cases, large energy gains resulted from only one or two interactions with the shock front. Scattering back to the shock from upstreams waves was observed much more frequently than scattering from downstream waves. For our simulations, the wave amplitude, and thus the diffusion coefficient, varies greatly with distance from the shock. A comparison of results from two different Mach number simulations showed the energetic particle fluxes are qualitatively consistent with the predictions of diffusive shock theory, although diffusive theory is not strictly applicable to these simulations. At higher energies, the fluxes fall off more rapidly than the diffusive theory prediction. This is probably due in part to the folding in of a spatial dependence of the energetic ion densities and in part due to the finite length and time of the simulation. To

run simulations large enough and long enough to accelerate particles to actual anomalous cosmic ray energies would be computationally prohibitive. Rather, the distribution of the energetic pick-ups found in simulations can be used as the “seed” population to inject into diffusive shock acceleration models which can then study the acceleration from the tens of keV energies found hereto the MeV anomalous cosmic ray range.

We wish to thank M. Lcc and D. Ellison for valuable discussions and Edith Huang, JPL, for assistance in using the Delta. This work was carried out at the Jet Propulsion Laboratory, California Institute of Technology, under a contract with the National Aeronautics and Space Administration. The research was supported in part by NASA/Heliospheric Physics and in part by NSF under Cooperative Agreement CCR-88809615. The computations were performed on the Intel Touchstone Delta parallel supercomputer operated for the Concurrent Supercomputing Consortium by the California Institute of Technology; access was provided by NASA.

## References

- Forman, M. A., and Webb, G. M., Acceleration of energetic particles, in *Collisionless Shocks in the Heliosphere: A Tutorial Review*, *Geophys. Monograph* 34, 91, (R. G. Stone and B. T. Tsurutani, eds.) AGU, 1985.
- Giacalone, J., Burgess, D., and Schwartz, S. J., Ion injection and acceleration at parallel shocks: comparisons of self-consistent plasma simulations with existing theories, *Astrophys. J.*, 402, 550, 1993.
- Giacalone, J., Burgess, D., and Schwartz, S. J., Hybrid simulations of protons strongly accelerated by a parallel collisionless shock, *Geophys. Res. letters*. 19, 433, 1992.
- Gloeckler, G., Geiss, J., Balsiger, H., Fisk, L., Galvin, A., Ipavich, F., Ogilvie, K., von Steiger, R., and Wilken, B., Detection of interstellar pick-up hydrogen in the solar system, (submitted for publication), 1993.
- Jokipii, J. R., Particle drift, diffusion, and acceleration at shocks, *Astrophys. J.*, 255, 716, 1982.

- Jokipii, J. R., Particle acceleration at a termination shock, 1, Application to the solar wind and the anomalous component, *J. Geophys. Res.*, 91, 2929, 1986.
- Jokipii, J. R., Rate of energy gain and maximum energy in diffusive shock acceleration, *Astrophys. J.*, 313, 842, 1987.
- Jokipii, J. R., The anomalous component of cosmic rays, in *Physics of the Outer Heliosphere*, 169, ed. by S. Grzedzielski and D. F. Page, COSPAR, Pergamon, Oxford, 1990.
- Jokipii, J. R., Kota, J., and Giacalone, J., Perpendicular transport in 1- and 2-dimensional shock simulations, *Geophys. Res. Lett.*, 20, 1759, 1993.
- Jones, F. C. and Ellison, D. C., The plasma physics of shock acceleration, *Space Sci. Revs.* 58, 259, 1991.
- Licwer, P. C., Goldstein, B. E., and Omid, N., Hybrid simulations of the effects of interstellar pick-up hydrogen on the solar wind termination shock, *J. Geophys. Res.* 98, 15,211, 1993.
- Pesses, M., Jokipii, J. R., and Eichler, D., Cosmic ray drift, shock wave acceleration, and the anomalous component of cosmic rays, *Astrophys. J. Lett.*, 246, 1.85, 1981.
- Scholer, M. Diffuse ions at quasi-parallel collisionless shocks: simulations, *Geophys. Res. Lett.*, 17, 1821, 1986.
- Winske, D., and Leroy, M. M., Hybrid simulations techniques applied to the earth's bow shock, in *Computer Simulation of Space Plasmas--Selected Lectures at the First ISSS*, ed. by H. Matsumoto and T. Sato, D. Ridel, Hingham, Mass., 1985.

### Figure Captions

**Fig. 1.** Results from Case 1 ( $\theta_{Bn} = 40^\circ$  and  $M_A = 5$ ) at times early (a) and late (b) in the simulation. Magnetic field y component  $B_y(x)/B_0$  vs. x, pick-up ion  $V_x$  vs. x phase space, (only every 60th particle plotted), and "energetic/reflected" pick up ion density  $n_{ref}^p$  (normalized to the upstream pick-up ion density  $n_{p0}^p$ ) where "energetic/reflected" pick-up ions are upstream ions with energy greater than 4 times the initial energy in the solar wind

frame. The upstream wave structure can be clearly seen in both  $B_y$  and the phase space of the "energetic/reflected" pick-up ions, which drive the waves.

Fig. 2. Power spectrum of the magnetic field fluctuations  $P(k)=B^2(k)/8\pi$  vs  $k$  for Case 1 at times early and late in the simulation with  $k$  in units of  $\omega_{pi}/c$ . The peak at early times agrees with predictions for a reflected pick-up ion beam-driven ion cyclotron instability.

Fig. 3. "Orbit" of two ions from Case 1. Plotted is the ion's energy ( $E=v^2/c^2$  in the solar wind frame) as a function of its distance from the shock front  $x-x_{shock}$  (negative values are upstream). The ion position and energy ( $E_0=5 \times 10^{-7}$ ) at the start of the simulation are at the bottom left end of the curve. The energy gain from shock drift acceleration is evident: the ions drift in the shock front ( $x-x_{shock} \approx 0$ ) and gain energy continuously.

Fig. 4. Energetic ion flux resulting from the acceleration processes and the diffusive shock theory predictions for Case 1 and Case 2. Plotted is the differential energy flux  $dJ(E)/dE$  of energetic/reflected ions in a region ( $x\omega_{pi}/c=0-1800$ ) upstream of the shock where  $E=v^2/c^2$ . The energetic flux resulting from the stronger shock (Case 2) leads to a broader distribution with a slower fall off with energy, consistent with diffusive theory predictions.

Fig. 5. Results from Case 2 ( $\theta_{Bn}=50^\circ$  and  $M_A=8$ ) late in the simulation. Magnetic field component  $B_y(x)/B_0$ , the total magnetic field strength  $B(x)/B_0$  and the "energetic/reflected" pick up ion density  $n_{ref}^P$ , normalized to the upstream pick-up ion density  $n_{P0}^P$ .

Fig. 6. Power spectrum of the magnetic field fluctuations  $P(k)=B^2(k)/8\pi$  vs  $k$  for Case 2 at times early and late in the simulation with  $k$  in units of  $\omega_{pi}/c$ .

Fig. 7. "Orbits" of two ions from Case 2. Plotted is the ion energy ( $E=v^2/c^2$  in the solar wind frame) as a function of distance from the shock front  $x-x_{shock}$  (negative values are upstream). Both ions have been accelerated to about 50 times their initial energy to  $E=6 \times 10^{-5}$ , corresponding to about 30 keV.

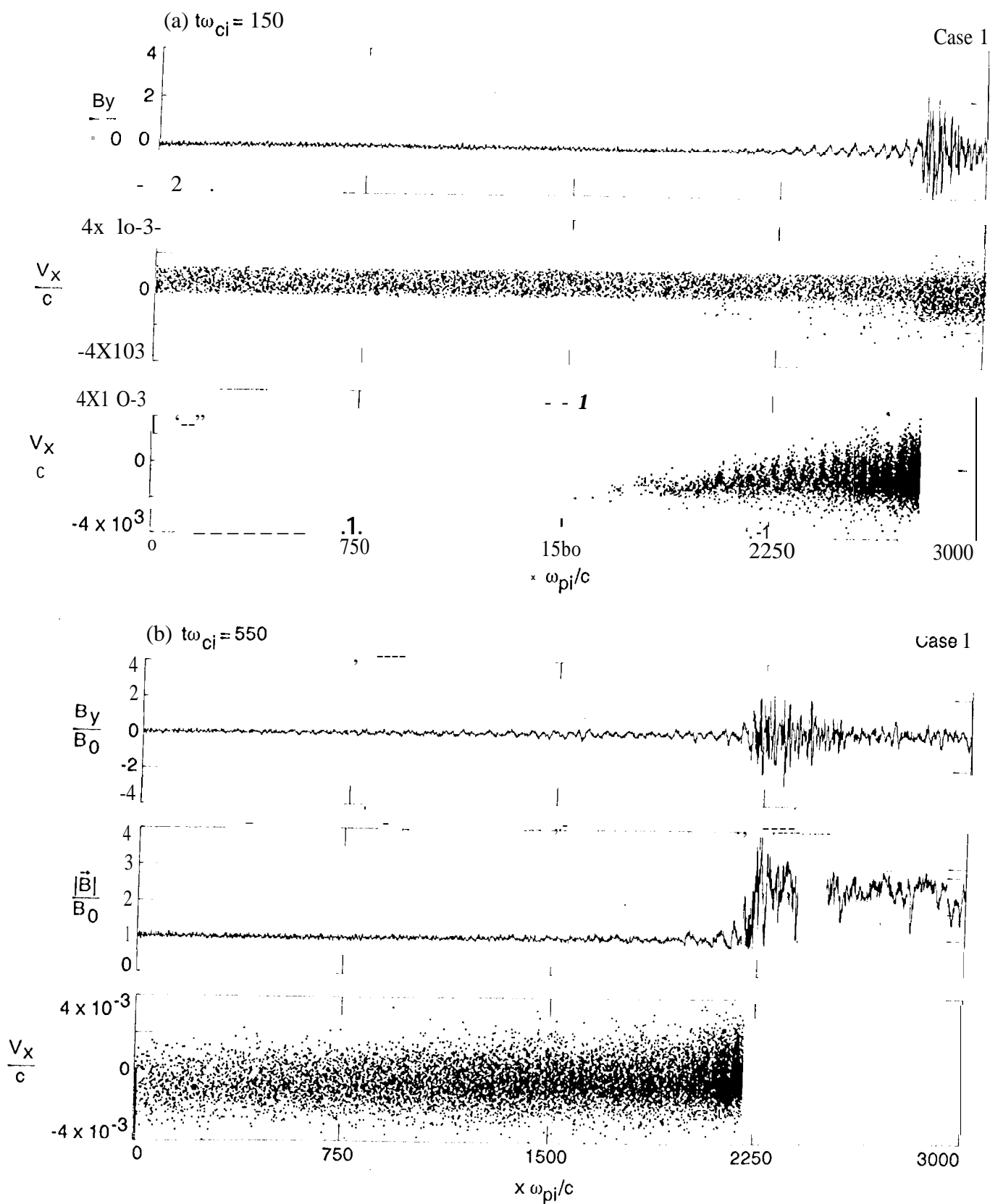


Fig.1

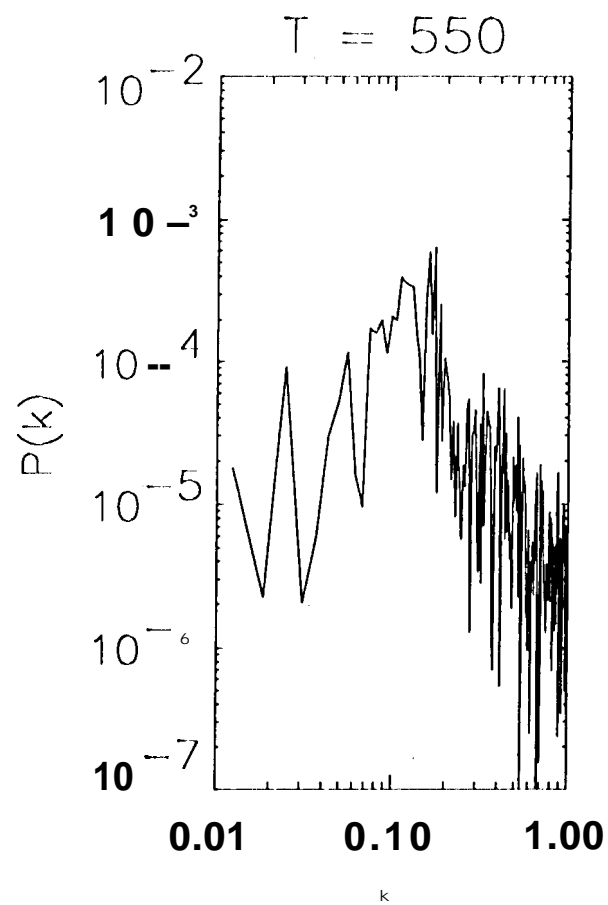
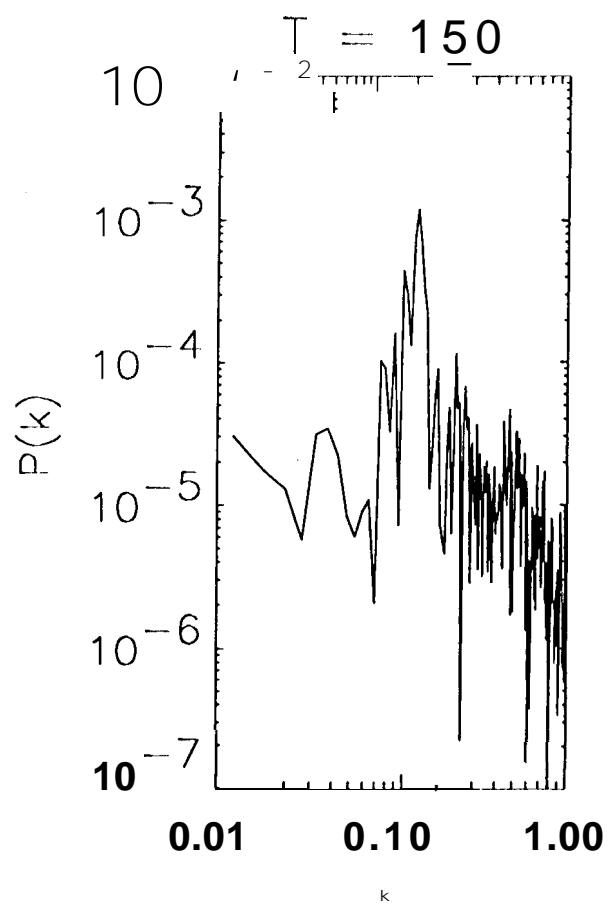


Fig. 2

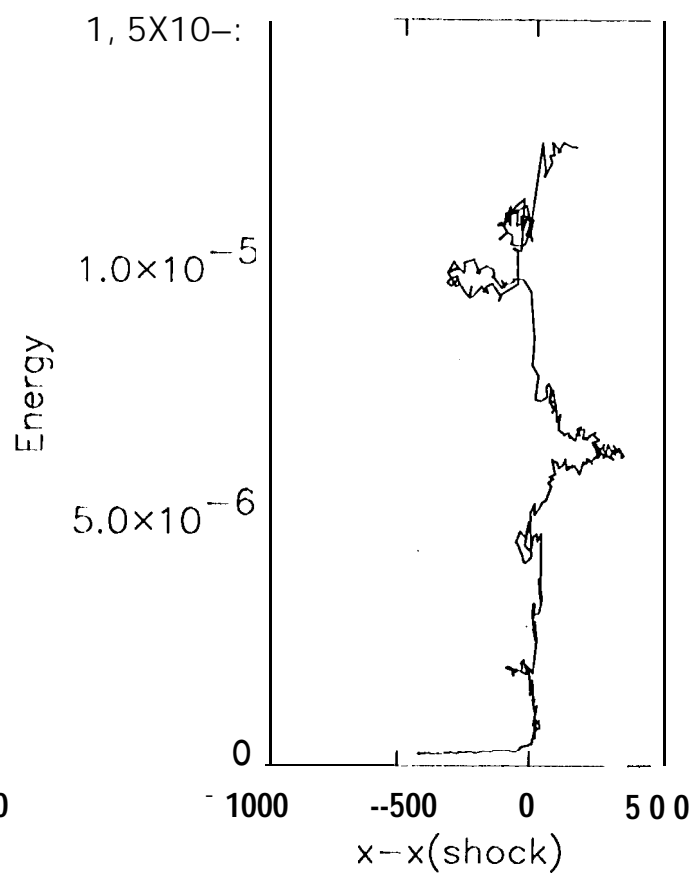
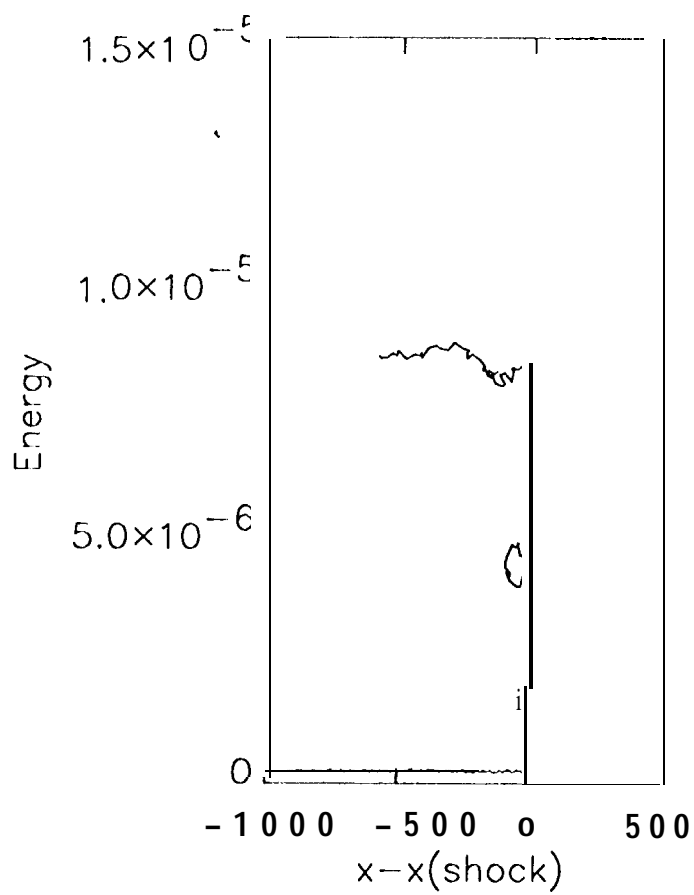


Fig. 3

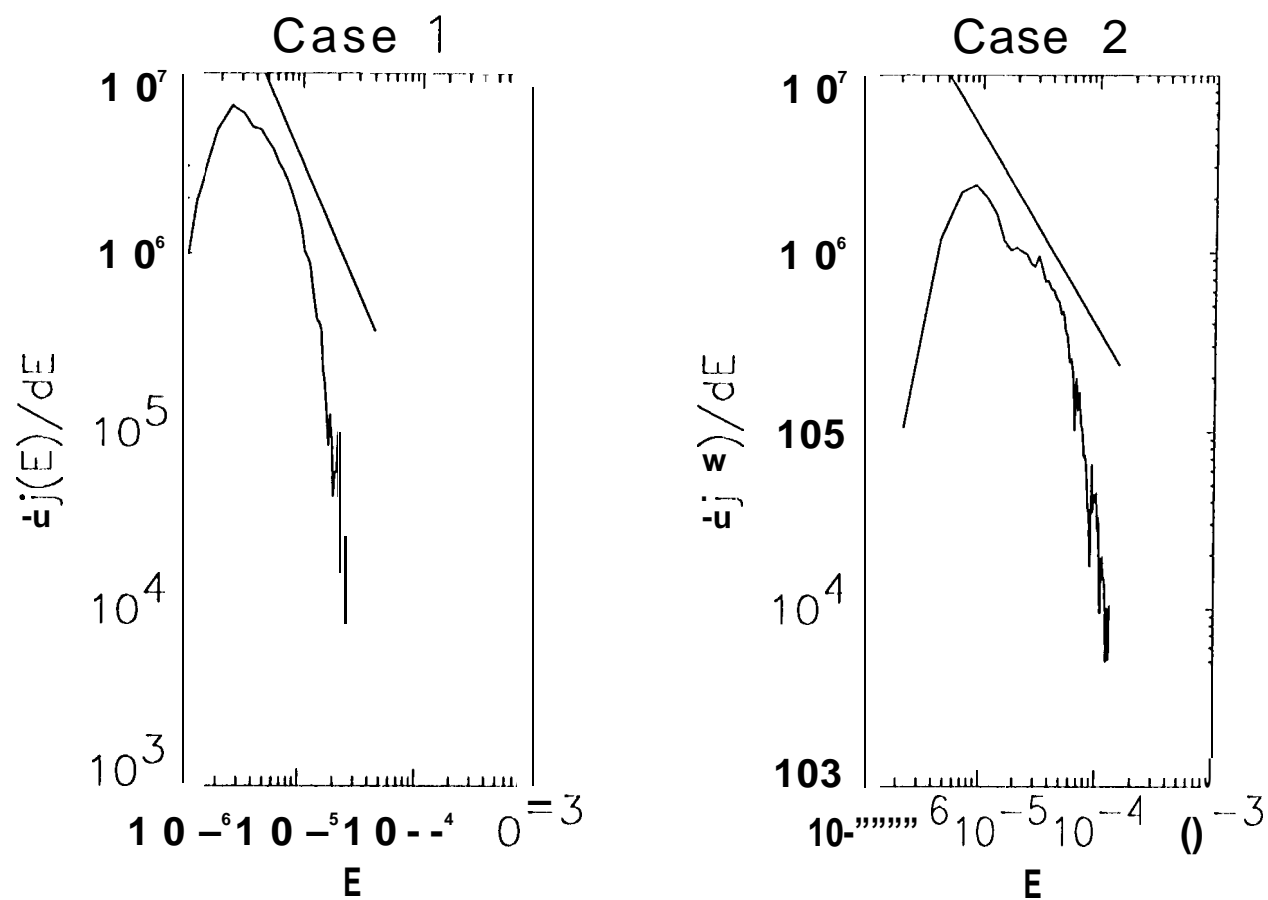


Fig. 4

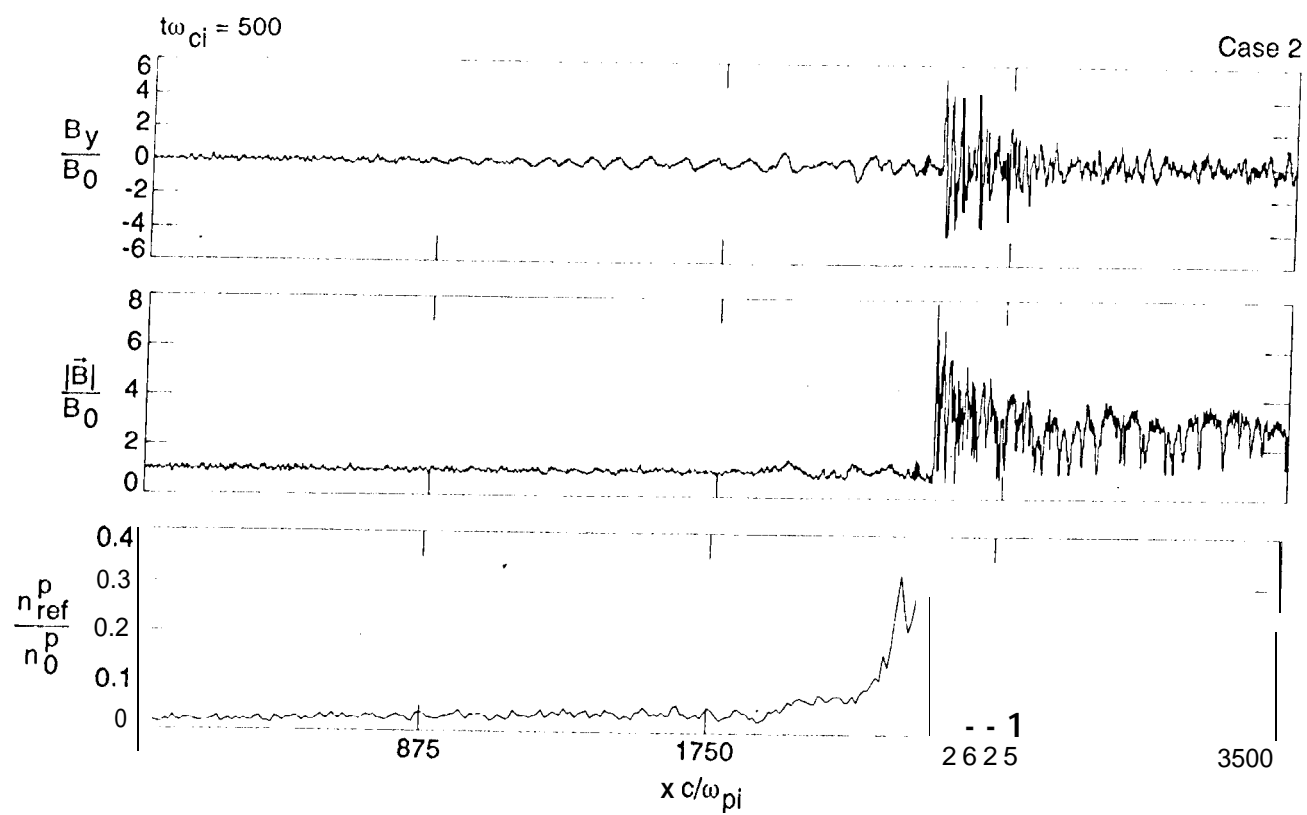


Fig. 5

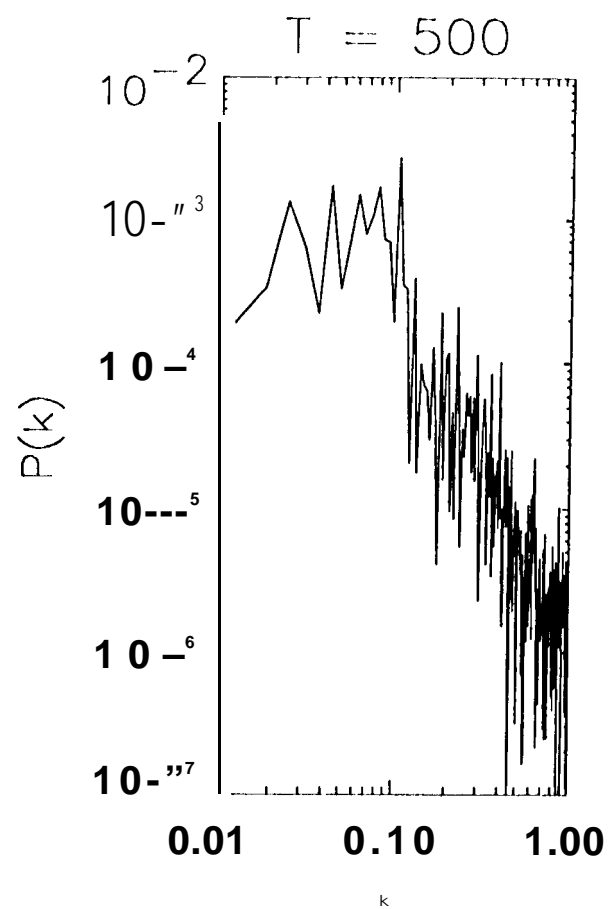
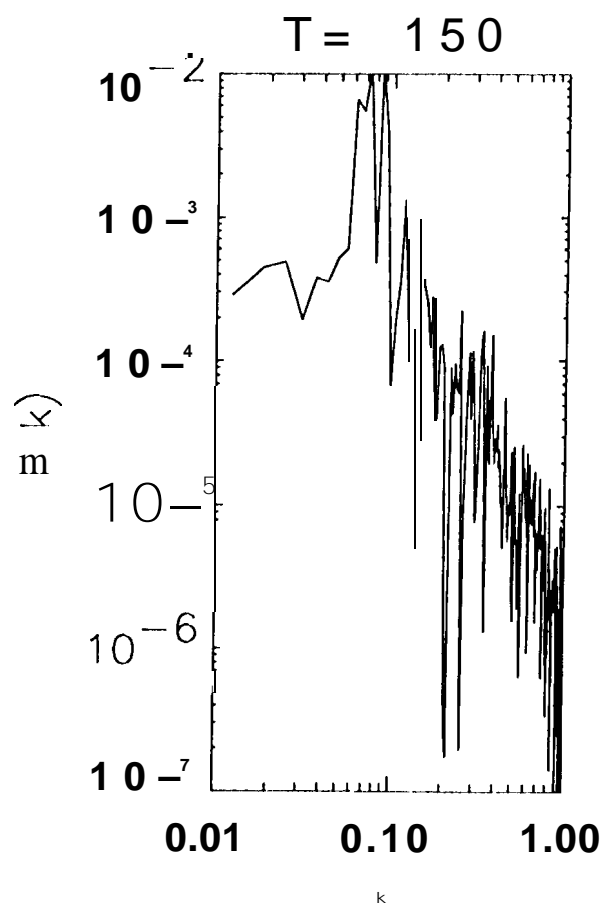


Fig. 6

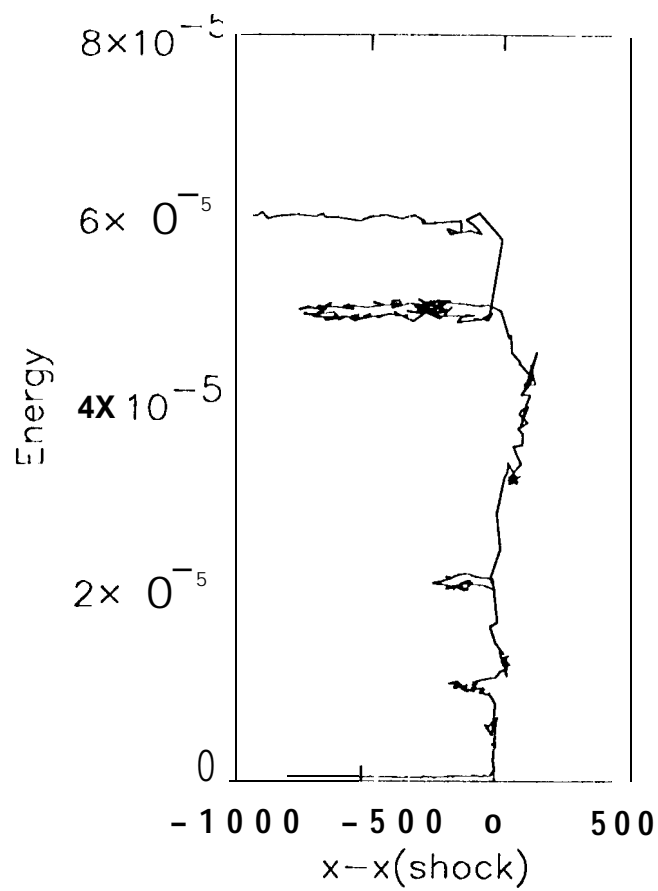
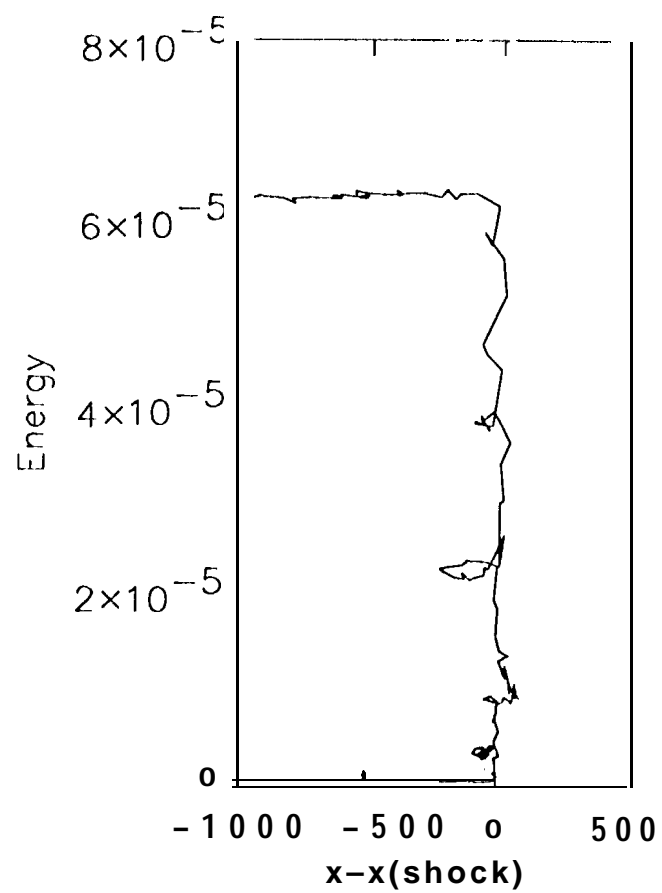


Fig. 7